Editors' Suggestion

Dielectric Constant of Liquid Water Determined with Neural Network Quantum Molecular Dynamics

Aravind Krishnamoorthy,[1] Ken-ichi Nomura,[1] Nitish Baradwaj,[1] Kohei Shimamura,[2] Pankaj Rajak,[3] Ankit Mishra,[1] Shogo Fukushima,[2] Fuyuki Shimojo,[2] Rajiv Kalia,[1] Aiichiro Nakano,[1] and Priya Vashishta[1,*]

[1]*Collaboratory for Advanced Computing and Simulations, Department of Chemical Engineering and Materials Science, Department of Physics & Astronomy, and Department of Computer Science, University of Southern California, Los Angeles, California 90089, USA*

[2]*Department of Physics, Kumamoto University, Kumamoto 860-8555, Japan*

[3]*Argonne National Laboratory, Lemont, Illinois 60439, USA*

(Received 24 December 2020; accepted 30 March 2021; published 25 May 2021; corrected 9 July 2021)

The static dielectric constant ε_0 and its temperature dependence for liquid water is investigated using neural network quantum molecular dynamics (NNQMD). We compute the exact dielectric constant in canonical ensemble from NNQMD trajectories using fluctuations in macroscopic polarization computed from maximally localized Wannier functions (MLWF). Two deep neural networks are constructed. The first, NNQMD, is trained on QMD configurations for liquid water under a variety of temperature and density conditions to learn potential energy surface and forces and then perform molecular dynamics simulations. The second network, NNMLWF, is trained to predict locations of MLWF of individual molecules using the atomic configurations from NNQMD. Training data for both the neural networks is produced using a highly accurate quantum-mechanical method, DFT-SCAN that yields an excellent description of liquid water. We produce 280×10^6 configurations of water at 7 temperatures using NNQMD and predict MLWF centers using NNMLWF to compute the polarization fluctuations. The length of trajectories needed for a converged value of the dielectric constant at 0°C is found to be 20 ns (40×10^6 configurations with 0.5 fs time step). The computed dielectric constants for 0, 15, 30, 45, 60, 75, and 90°C are in good agreement with experiments. Our scalable scheme to compute dielectric constants with quantum accuracy is also applicable to other polar molecular liquids.

DOI: 10.1103/PhysRevLett.126.216403

The large dielectric constant of liquid water, $\varepsilon_0 \cong 78$ at room temperature [1], plays a crucial role in determining its physical and chemical behavior. This large dielectric constant is also responsible for the excellent solvation properties of water and its importance in biological systems. Predicting the dielectric constant of water has long been a challenge for quantum theory. Simulations and theory at various levels of sophistication have been used over decades to compute ε_0 for liquid water. However, a fully quantum mechanical calculation of the dielectric constant without any *ad hoc* assumptions regarding structural correlations in water has not been possible yet. The primary challenge in obtaining ε_0 from quantum simulations is the requirement for very long (tens of nanoseconds) trajectories, to accurately compute polarization fluctuations to compute ε_0, which are out of reach even on a petascale supercomputer using quantum molecular dynamics.

After the seminal paper on water in 1933 by Bernal and Fowler [2], the first attempt to compute dielectric constant of liquid water in 1951, was made by Pople [3], who adapted Kirkwood's theory [4] by postulating that the main effect of liquid disorder was to bend the hydrogen bonds while the fourfold ice coordination was preserved. This is reflected in the r-dependent Kirkwood G factor $G_K(r)$, which is an orientational correlation function for molecular dipoles (r is interatomic distance) [5]. By adopting a distribution of the bending angles to fit the pair-correlation function obtained from x-ray experiments in the 1930s, Pople estimated the correlation factor $G_K(r)$ to be ~2.5. This yielded a dielectric constant of ~64, in fairly good agreement with experiment. After the invention of the molecular dynamics (MD) method in 1964 by Rahman [6], and the pioneering study of aqueous solutions by Rahman and Stillinger [7], it has been possible to compute the dielectric response of water using classical MD, but with rather limited success. Most computer simulations of water for dielectric properties are performed using empirical potential functions with point charges that do not account for many-body induced polarization effects explicitly [8]. Owing to these approximations, MD simulation of the dielectric constant remains challenging [9–13], especially at low temperatures. Factors such as the interatomic potential [14,15] and length of MD trajectory needed for the convergence are serious limitations [16].

Recently, neural networks and the radial and angular feature vectors introduced by Behler and Parrinello [17–25]

 © 2021 American Physical Society

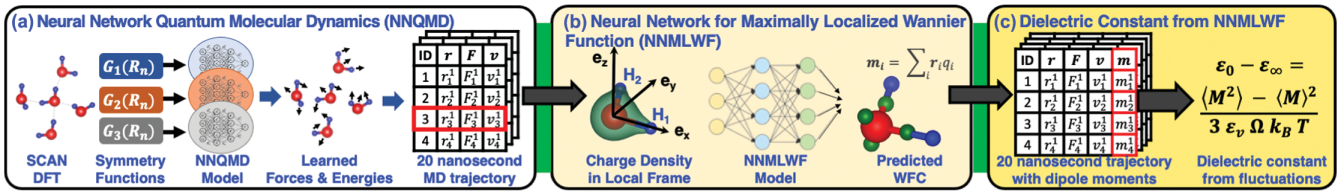

FIG. 1. Dielectric constant computation involves linking. (a) Neural networks trained on DFT-SCAN configurations to produce 280×10^6 time step NNQMD trajectory with (b) training a deep neural network for MLWF locations and predicting the MLWF centers for the 280×10^6 time step trajectory. (c) Polarization fluctuations are computed for configurations over a 20 ns long NNQMD trajectory for each temperature to calculate the dielectric constant for liquid water.

can model the potential energy surface and forces of a multicomponent system upon training with QMD data produced within density functional theory (DFT) with a suitable exchange-correlation function. Such machine learning methods have been successfully used for defect migration, structural stability, and many properties on material and chemical systems [26–31]. Marzari and Vanderbilt [32] in 1997 proposed maximally localized Wannier functions (MLWF), which are obtained as a unitary transformation that minimizes the spread of ground-state DFT Kohn-Sham orbitals [33] for computing polarization and implemented their method into electronic structure codes. Great strides have been made by Parrinello, Car, Galli, and Gygi [34–37] and collaborators to compute polarization in liquid water using MLWF and the r-dependent Kirkwood G factor $G_K(r)$. Important advances were made by Car and collaborators in using neural networks to fit DFT computed MLWFs for water and using these to predict trajectories for the computation of infrared spectra [38–41].

We propose an end-to-end scheme that uses only atomic coordinates, energies, and forces for a deep neural network training and the second neural network to map input atomic coordinates into output MLWF locations. The proposed scheme is size extensive, preserves translational, rotational, and permutational symmetries, and yields a converged value of the polarization fluctuation, given sufficiently long trajectory.

Figure 1 shows the steps involved in the computation of the dielectric constant using the two deep neural networks. There are seven steps in our computation of ε_0 for liquid water. (i) Computation of QMD trajectories for several temperature-density conditions for an exhaustive sampling of the potential energy surface and forces. Since these data will be used to train both neural networks in the dielectric constant scheme, it is critical to perform QMD simulations that accurately reflect the potential energy surface based on the DFT where exchange-correlation effects are incorporated by the highly accurate SCAN functional [42]. A 216 molecule system of liquid water is run using a DFT-SCAN in an NVT ensemble for 40 000 time steps under a variety of density and temperature conditions. (ii) Training of a deep neural network with two hidden layers using 52-dimensional rotationally and translationally invariant 32×10^6 feature vectors. The quality of NNQMD training is tested on a 41 472 atom and 1 119 744 atom water systems by computing structural and dynamical correlations (Fig. 2). (iii) Using NNQMD, we compute 40×10^6 time steps (with a time step of 0.5 fs) at 7 temperatures from 0°C to 90°C for a total of 280×10^6 steps. (iv) MLWF and their locations are computed for 3000 DFT-SCAN configurations for training the second deep neural network, NNMLWF. (v) This deep neural network is then used to predict the locations of MLWF for 56×10^6 NNQMD configurations. (vi) For each temperature NNMLWF predicted configurations are used to compute $\langle M^2 \rangle$ and $\langle M \rangle^2$ to determine ε_0. (vii) ε_∞ is computed using the Berry phase method for liquid water configurations and averages are performed to get an ensemble average [43–45].

We use the ænet method for training energies and forces [18]. In this work, as the fitting algorithm, the limited-memory Broyden-Fletcher-Goldfarb-Shanno method was employed. We used a neural network consisting of two hidden layers with modified scaled hyperbolic tangent [18] as the activation function [46].

The DFT simulations [54,55] using local functionals like the generalized gradient approximation (GGA) [56–58] have been used to understand high-pressure, confined, and reacting phases of water, but liquid water presents a major challenge in the choice of exchange-correlation function. Perdew and Klein and their collaborators have demonstrated that a meta-GGA based on the SCAN functional [42] captures the density difference between ice and water at ambient conditions and predicts structural, electronic, and dynamic properties of liquid water in good agreement with experiments.

Our approach extends the spatial dimensions of the systems and the length of time trajectories not achievable by QMD simulations. It is therefore possible to study structural and dynamical correlations, rare events, such as crystal nucleation [59], with enhanced sampling methodologies in simulations of QMD quality at a cost that is several orders of magnitude lower. On the current petascale supercomputers, it is possible to investigate billion atom systems and for microsecond timescales.

In NNQMD simulations with periodic boundary conditions, the dielectric constant of an isotropic and

homogeneous fluid can be calculated using the fluctuation formula [39,60,61],

$$\varepsilon_0 = \varepsilon_\infty + \frac{4\pi}{3k_B T\ \Omega}(\langle M^2\rangle - \langle M\rangle^2), \tag{1}$$

where ε_0 is the static dielectric constant, T is temperature, Ω is volume. and $\langle\ \rangle$ denote the canonical ensemble averages. The total polarization is given as $M = \sum_i \mu_i$ [62]. The higher dielectric constant of water can be associated with the presence of a H-bond network [39]. Owing to the complexity of the H-bond network and its competition with thermal fluctuations, a molecular-level understanding of the structure of water remains elusive [63]. The presence of hydrogen bonding slows down dipolar fluctuations and leads to longer convergence times. The high cost of evaluation of Eq. (1) has been a strong motivation for the development for an efficient approach using deep neural network based NNQMD and NNMLWF simulation methods.

MD simulations using empirical potentials have shown that trajectories longer than 10 ns are necessary for the convergence of dielectric constant [64,65]; these are not practically feasible with QMD simulations. NNQMD produces quantum-accurate trajectories for liquid water that are sufficiently long to capture dielectric relaxation and reorientation of the H-bond network and enable accurate computation of the dielectric constant.

Figure 2 shows the radial distribution functions $g(r)$, and bond-angle distributions of liquid water generated by NNQMD simulations. The $g(r)$ for H—H, O—H, and O—O [Figs. 2(a), 2(c), and 2(e)] show that NNQMD reproduces the intramolecular O—H bond length as well as the radial position of the second and third solvation shells. The intramolecular H—O—H bond-angle distribution involving only covalent bonds (CB) [Fig. 2(d)] agrees well with the DFT-SCAN internal angle of 105°. More importantly, the distributions for intermolecular bond angles, O—H$\cdots$O involving the CB and H bond, and the H$\cdots$O$\cdots$H angle involving both H bonds, where single dash indicates CB at 0.97 Å and double dash indicates H bond at 1.75 Å, are also in good agreement with the ground truth.

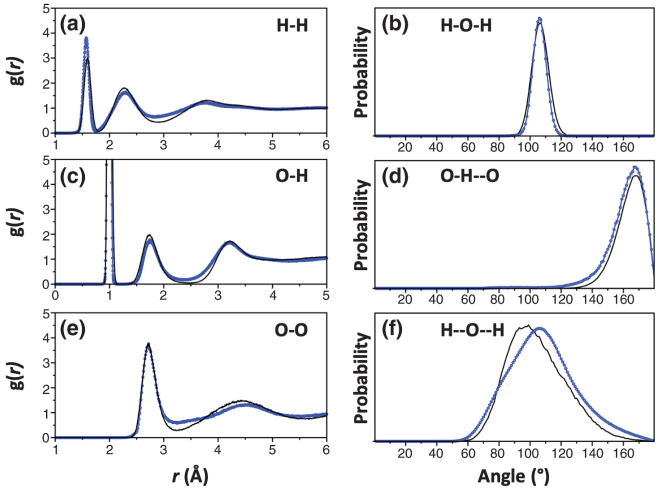

FIG. 2. (a),(c),(e) Comparison of pair distribution functions $g(r)$ for H—H, O—H, and O—O from DFT-SCAN (black) and NNQMD (blue) at 30 °C. (b),(d),(f) Distributions of the intramolecular H—O—H angle with both the CB and O—H——O angle with CB and H bond, and the H—O—H angle with both H bonds between DFT-SCAN and NNQMD. NNQMD reproduces structural details of liquid water. The single dash is covalent bond 0.97 Å and the double dash is the H bond at 1.75 Å. DFT-SCAN results for $g(r)$ are in excellent agreement with neutron experiments.

There is no direct method to experimentally determine the H-bond lifetime [66]. For example, vibrational relaxation times of 0.74 ps have been reported for water [67], whereas observed rotational relaxation times range from 0.6 [68] to 2.1 ps [69]. A computational estimate of H-bond lifetimes largely depends on the definition of the H bond [66]. In our investigation, we use the joint angle-distance criterion, where the intermolecular O—H distance r_{OH} is less than $\mathrm{C}^1_{\mathrm{OH}} + \mathrm{C}^2_{\mathrm{OH}}\cos\theta$, where θ is the angle between one oxygen and two inter- and intramolecule hydrogen atoms. $\mathrm{C}^1_{\mathrm{OH}}$ and $\mathrm{C}^2_{\mathrm{OH}}$ are parameters depending on the phase of water [70]. For room temperature water $\mathrm{C}^1_{\mathrm{OH}} = 1.37$ (Å) and $\mathrm{C}^2_{\mathrm{OH}} = -1.71$ (Å) are used. We compute H-bond lifetimes using the population time correlation function,

$$C(t) = \frac{1}{N^{t=0}_{\mathrm{HB}}}\sum_{i=1}^{N_W}\sum_{j<i}^{N_W} h_{ij}(0)h_{ij}(t), \tag{2}$$

where N_W is the number of water molecules in the simulation, $N^{t=0}_{\mathrm{HB}}$ is the number of H bonds at $t = 0$ [71].$h_{ij}(t)$ is the H-bond state function, which is unity as long as the pair of molecules i and j remain H bonded. The function becomes zero and remains zero after the first time the H bond is broken. Figure 3 shows the H-bond population correlation from NNQMD trajectories. Validation is provided from QMD. The NNQMD decay time at 30°C of 0.976 ps agrees with the range of values, 0.6–2.1 ps from experiments.

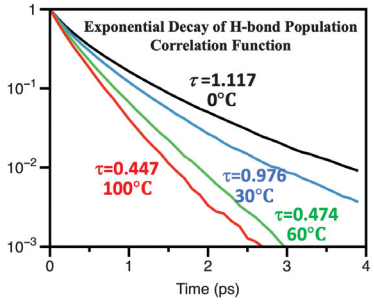

H-bond Decay Time (τ)

Temp. (°C)	QMD (ps)	NNQMD (ps)
0	0.993	1.117
30	0.927	0.976
60	0.468	0.474
90	0.390	0.447

FIG. 3. Time decay of the H-bond population correlation in water as a function of temperature from NNQMD. NNQMD is validated with QMD, as shown in the table.

From the NNQMD liquid water configurations we compute the dipole moment, $\vec{M}$, that is the sum of molecular moments calculated using the MLWF centers. The dipole moment of a single water molecule comes from the summation of $q\vec{r}_{ij}$ where $\vec{r}_{ij}$ is the vector pointing from the position of the MLWF centers and the position of the hydrogen to the oxygen in the individual water molecule. The charges, q, of the MLWF centers are -2 and atomic site of H is $+1$ and O is $+6$.

The quantum computation of MLWF centers for millions of configurations is intractable even on petascale supercomputers. We use a deep neural network, NNMLWF, that predicts the location of MLWF centers for individual water molecules using the coordinates of atoms in the molecule and its surroundings [35] within the local frame of the molecule. We use a relatively short range for the NNMLWF feature vector as a consequence of the principle of nearsightedness of electronic matter [60,61]. The NNMLWF is trained on MLWF centers computed for 3000 liquid water configurations generated from a DFT-SCAN. NNMLWF uses symmetry preserving smooth feature vectors by transforming them to the molecular frame from the laboratory frame by a unitary transformation. The NNMLWF model can predict the location of the four MLWF centers in the molecular frame that are then transformed back into the laboratory frame by performing the reverse unitary transformation, with an accuracy of 0.025 Å. This scalable NNMLWF scheme can therefore be applied to millions of independent configurations from NNQMD. Initially, the DFT-SCAN is used to train the NNQMD model, which generates 20 ns trajectory of liquid water for each temperature. These configurations are then provided as inputs to NNMLWF, which predicts the location of MLWF centers for each water molecule in each configuration. These MLWF centers are used to compute the dipole moments for molecules that are then summed up to get the polarization for the configuration of liquid water, whose fluctuations in the canonical ensemble is then used to calculate the dielectric constant.

The positions of the four MLWF [33,72] of a water molecule are along the two covalent O—H bonds and on two lone pairs of oxygen, which is in the direction of the hydrogen bonds. Figure 4 shows the distribution of the dipole moments of water molecules computed using the NNMLWF compared to the distribution of dipole moments computed from MLWF computed with DFT-SCAN, the ground truth. Individual molecular moments in water are not experimentally accessible, reflecting a basic arbitrariness in partitioning the electronic charge between individual molecules in a condensed environment [38,73]. In this context, experimental estimates such as 2.9 ± 0.6 D [74] based on the measured x-ray form factor of liquid water, or theoretical estimates based on various partitioning schemes [34,75,76], should be only taken as reasonable estimates. For isolated water molecules, the MLWF based

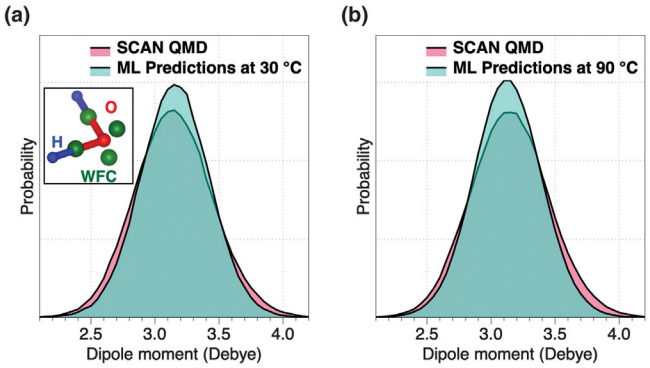

FIG. 4. The distribution of molecular dipole moments computed from the MLWF centers prediction from NNMLWF and the distribution of moments from DFT-SCAN, the ground truth. (a) 30°C and (b) 90°C. The value of mean and standard deviation between the two distributions validates the use of NNMLWF for the computation of the dielectric constant. (Inset) Centers of MLWF (green) in an isolated water molecule are localized along the O—H bonds and on the sp^3 lone pairs on the O atom.

on a DFT-SCAN gives a dipole moment of 2.2 D, whereas most sophisticated configuration interaction (CI) theory [77] gives a value 1.854 D that is in excellent agreement with the experimental value of 1.855 D [78]. The discrepancy between DFT-SCAN value, 2.2 D, and the experimental value that is in excellent agreement with CI value, 1.854 D [78], is a result of three approximations in all DFT based electronic structure calculations: (i) the local density approximation in DFT, (ii) pseudopotential approximation versus all electron computation in CI, and (iii) approximation of transforming the full electronic charge density into MLWFs. These three approximations result in an error of about 18% over estimation in the predicted DFT-SCAN dipole moment of an isolated water molecule, which leads to an 18% over estimation of computed polarization $\vec{M}$.

Once the NNMLWF is validated, we compute the dipole moment correlations from 20 ns NNQMD trajectory. The formula used to calculate the dielectric constant is

$$\varepsilon_0 - \varepsilon_\infty = \frac{4\pi\,\Delta M^2}{\varepsilon_{\rm vac} 3\Omega k_B T},$$

where $\Delta M^2 = \langle M^2\rangle - \langle M\rangle^2$ and $M(t) = \sum_j^{N_{\rm Mol}} \sum_\alpha^{N_{\rm atom}} [r_{\alpha j}(t) - r_{0j}(t)] q_{\alpha j}$, where $N_{\rm atom}$ is the number of H atoms and MLWF centers in the molecule j. $q_{\alpha j}$ is the charge on atom α, $r_{\alpha j}$ is the position of the MLWF centers and r_{Hj} location of H atoms and r_{0j} is the position of the O atom. We have computed the high-frequency dielectric constant, ε_∞ to be 1.79, consistent with experiments [79]. Results are shown in Fig. 5.

The dielectric constant is computed for 7 temperatures in between 0°C to 90°C. Fluctuations are computed from the configurations every 20 fs apart along the NNMLWF

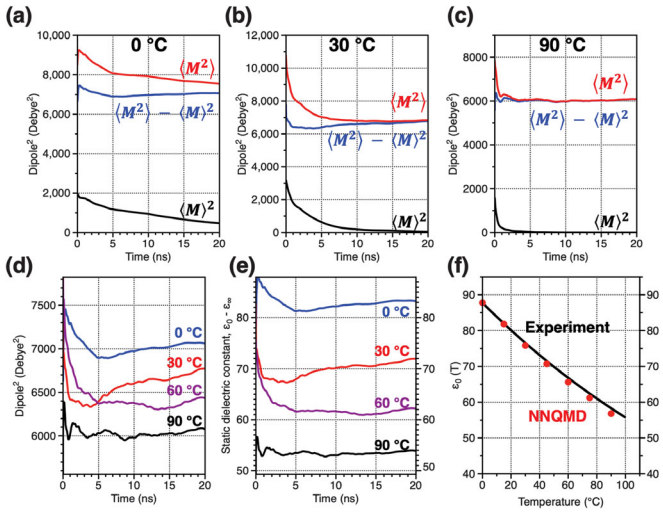

FIG. 5. (a)–(c) Computed values of $\langle M^2\rangle, \langle M\rangle^2$ and $\langle M^2\rangle - \langle M\rangle^2$ from NNMLWF prediction of MLWF centers from NNQMD trajectories of liquid water at 0, 30, and 90°C. The dielectric constant value depends upon the value of $\langle M^2\rangle - \langle M\rangle^2$, which converges at 20 ns, which is well beyond the scope of QMD trajectories. (d) $\langle M^2\rangle - \langle M\rangle^2$ values at four temperatures. (e) Computed dielectric constant of water at 273 and 363 K using the fluctuation formula in canonical ensemble. (f) Temperature dependence of NNQMD and NNMLWF computed dielectric constants are consistent with the experimentally values.

trajectory. Previous MD simulations with empirical potentials have shown that the computed fluctuations and the resulting dielectric constant values are independent of the frequency of sampling from 1 fs up to 100 fs [64].

Dielectric properties of water require extremely long configuration space trajectories due to a slow reorientational relaxation rate in the H-bond network [62,80]. The time required for convergence varies dramatically with temperature from <5 ns at 90°C to >20 ns at 0°C, as shown in Figs. 5(a)–5(c). It should be pointed out that the values of polarization, M, have been scaled down by 18% to accommodate the inherent shortcomings of DFT implementation with the best possible choice of exchange-correlation potential SCAN, the pseudopotential for H and O, and the implementation of MLWF to represent the total electronic charge density. Figure 5(d) shows that the computed values of the dielectric constant are consistent with experimental values of dielectric constant of liquid water in the range of 0−100°C [81,82] using a RF resonator to an accuracy of 0.2%.

The simulations presented here do not consider the nuclear quantum effects [83,84]. This is because *ab initio* path integral molecular dynamics is computationally too expensive to obtain 20 + ns long trajectories and NQE have relatively small effect on the dipole moment in water [85]. However, it should be pointed out that the dielectric constant of H_2O (78.45) and D_2O (78.08) at 25°C are practically identical in value [1], implying that the quantum effects in the motion of hydrogen are negligibly small for the dielectric constant of water.

The system size dependence of the dielectric constant is rather small, which is advantageous for QMD. Previous studies have shown that the dielectric constant value computed for a system size of 108 molecules [62,80] and 216 molecules is consistent with values computed from a 20 000 molecule system [64].

In summary, we have constructed a physics-based integrated approach for the computation of the dielectric constant of a polar fluid that combines two deep neural networks, NNQMD and NNMLWF. The approach combines the quantum mechanical accuracy of QMD and the computational efficiency of empirical potential models to compute the dielectric constant of water, ε_0. The accuracy of our method depends on judicious choice of a deep neural network and on the quality of the training data, which can be further improved by using improved exchange-correlation functionals beyond SCAN, which will produce the dipole moment of an isolated water molecule in agreement with the experimental data.

This work was supported as part of the Computational Materials Sciences Program funded by the U.S. Department of Energy, Office of Science, Basic Energy Sciences, under Award No. DE-SC0014607. This research was partly supported by Aurora Early Science programs and used resources of the Argonne Leadership Computing Facility, which is a DOE Office of Science User Facility supported under Contract No. DE-AC02-06CH11357. Computations were performed at the Argonne Leadership Computing Facility under the DOE INCITE and Aurora Early Science programs and at the Center for Advanced Research Computing of the University of Southern California.

*priyav@usc.edu

[1] K. R. Srinivasan and R. L. Kay, J. Chem. Phys. **60**, 3645 (1974).
[2] J. D. Bernal and R. H. Fowler, J. Chem. Phys. **1**, 515 (1933).
[3] J. A. Pople, Proc. R. Soc. A **205**, 163 (1951).
[4] J. G. Kirkwood, J. Chem. Phys. **7**, 911 (1939).
[5] M. Neumann, Mol. Phys. **50**, 841 (1983).
[6] A. Rahman, Phys. Rev. **136**, A405 (1964).
[7] A. Rahman and F. H. Stillinger, J. Chem. Phys. **55**, 3336 (1971).
[8] A. Shekhar, R. K. Kalia, A. Nakano, P. Vashishta, C. K. Alm, and A. Malthe-Sorenssen, Appl. Phys. Lett. **105**, 161907 (2014).
[9] J. Kolafa and L. Viererblova, J. Chem. Theory Comput. **10**, 1468 (2014).
[10] I. R. Iukhnovskii and M. F. Golovko, *Statistical Theory of Classical Equilibrium Systems* (Naukova Dumka, Kiev, 1980).
[11] D. J. Adams, Nature (London) **293**, 447 (1981).
[12] G. Raabe and R. J. Sadus, J. Chem. Phys. **134**, 234501 (2011).

[13] J. Alejandre, G. A. Chapela, H. Saint-Martin, and N. Mendoza, Phys. Chem. Chem. Phys. **13**, 19728 (2011).
[14] P. Zarzycki and B. Gilbert, Phys. Chem. Chem. Phys. **22**, 1011 (2020).
[15] J. Cardona, M. B. Sweatman, and L. Lue, J. Phys. Chem. B **122**, 1505 (2018).
[16] D. van der Spoel, P. J. van Maaren, and H. J. C. Berendsen, J. Chem. Phys. **108**, 10220 (1998).
[17] J. Behler and M. Parrinello, Phys. Rev. Lett. **98**, 146401 (2007).
[18] N. Artrith and A. Urban, Comput. Mater. Sci. **114**, 135 (2016).
[19] N. Artrith, T. Morawietz, and J. Behler, Phys. Rev. B **83**, 153101 (2011).
[20] V. L. Deringer, M. A. Caro, and G. Csanyi, Adv. Mater. **31**, 1902765 (2019).
[21] V. Botu, R. Batra, J. Chapman, and R. Ramprasad, J. Phys. Chem. C **121**, 511 (2017).
[22] B. Sanchez-Lengeling and A. Aspuru-Guzik, Science **361**, 360 (2018).
[23] T. Morawietz and J. Behler, J. Phys. Chem. A **117**, 7356 (2013).
[24] F. C. Mocanu, K. Konstantinou, T. H. Lee, N. Bernstein, V. L. Deringer, G. Csanyi, and S. R. Elliott, J. Phys. Chem. B **122**, 8998 (2018).
[25] E. D. Cubuk, S. S. Schoenholz, J. M. Rieser, B. D. Malone, J. Rottler, D. J. Durian, E. Kaxiras, and A. J. Liu, Phys. Rev. Lett. **114**, 108001 (2015).
[26] A. D. Sendek, Q. Yang, E. D. Cubuk, K. A. N. Duerloo, Y. Cui, and E. J. Reed, Energy Environ. Sci. **10**, 306 (2017).
[27] C. Draxl and M. Scheffler, MRS Bull. **43**, 676 (2018).
[28] M. Misawa, S. Fukushima, A. Koura, K. Shimamura, F. Shimojo, S. Tiwari, K.-i. Nomura, R. K. Kalia, A. Nakano, and P. Vashishta, J. Phys. Chem. Lett. **11**, 4536 (2020).
[29] S. Fukushima, E. Ushijima, H. Kumazoe, A. Koura, F. Shimojo, K. Shimamura, M. Misawa, R. K. Kalia, A. Nakano, and P. Vashishta, Phys. Rev. B **100**, 214108 (2019).
[30] K. Shimamura, S. Fukushima, A. Koura, F. Shimojo, M. Misawa, R. K. Kalia, A. Nakano, P. Vashishta, T. Matsubara, and S. Tanaka, J. Chem. Phys. **151**, 124303 (2019).
[31] P. Rajak, K. Liu, A. Krishnamoorthy, R. Kalia, A. Nakano, K.-I. Nomura, S. Tiwari, and P. Vashishta, in *Scalable Deep Learning over Parallel And Distributed Infrastructures, New Orleans, Louisiana, USA* (Institute of Electrical and Electronics Engineers (IEEE), New York, 2020).
[32] N. Marzari and D. Vanderbilt, Phys. Rev. B **56**, 12847 (1997).
[33] N. Marzari, A. A. Mostofi, J. R. Yates, I. Souza, and D. Vanderbilt, Rev. Mod. Phys. **84**, 1419 (2012).
[34] P. L. Silvestrelli and M. Parrinello, Phys. Rev. Lett. **82**, 3308 (1999).
[35] L. F. Zhang, M. H. Chen, X. F. Wu, H. Wang, E. Weinan, and R. Car, Phys. Rev. B **102**, 041121 (2020).
[36] C. Zhang, D. Donadio, F. Gygi, and G. Galli, J. Chem. Theory Comput. **7**, 1443 (2011).
[37] A. P. Gaiduk, F. Gygi, and G. Galli, J. Phys. Chem. Lett. **6**, 2902 (2015).
[38] M. Sharma, R. Resta, and R. Car, Phys. Rev. Lett. **95**, 187401 (2005).
[39] M. Sharma, R. Resta, and R. Car, Phys. Rev. Lett. **98**, 247401 (2007).
[40] G. M. Sommers, M. F. C. Andrade, L. F. Zhang, H. Wang, and R. Car, Phys. Chem. Chem. Phys. **22**, 10592 (2020).
[41] M. Boero, K. Terakura, T. Ikeshoji, C. C. Liew, and M. Parrinello, Phys. Rev. Lett. **85**, 3245 (2000).
[42] J. W. Sun, A. Ruzsinszky, and J. P. Perdew, Phys. Rev. Lett. **115**, 036402 (2015).
[43] P. Umari and A. Pasquarello, Phys. Rev. Lett. **89**, 157602 (2002).
[44] I. Souza, J. Iniguez, and D. Vanderbilt, Phys. Rev. Lett. **89**, 117602 (2002).
[45] F. Shimojo *et al.*, SoftwareX **10**, 100307 (2019).
[46] See Supplemental Material at http://link.aps.org/supplemental/10.1103/PhysRevLett.126.216403 for description of deep neural network training, which includes Refs. [47–53].
[47] K. Lee, D. Yoo, W. Jeong, and S. Han, Comput. Phys. Commun. **242**, 95 (2019).
[48] A. Singraber, T. Morawietz, J. Behler, and C. Dellago, J. Chem. Theory Comput. **15**, 3075 (2019).
[49] L. F. Zhang, J. Q. Han, H. Wang, R. Car, and E. Weinan, Phys. Rev. Lett. **120**, 143001 (2018).
[50] K. Yao, J. E. Herr, David W. Toth, R. McKintyre, and J. Parkhill, Chem. Sci. **9**, 2261 (2018).
[51] J. Behler, Int. J. Quantum Chem. **115**, 1032 (2015).
[52] J. Behler, J. Chem. Phys. **134**, 074106 (2011).
[53] L. Zhang, J. Han, H. Wang, W. A. Saidi, R. Car, and E. Weinan, Nips'18, 4441 (2018).
[54] P. Hohenberg and W. Kohn, Phys. Rev. **136**, B864 (1964).
[55] W. Kohn and P. Vashishta, in *Theory of the Inhomogeneous Electron Gas*, edited by S. Lundqvist and N. H. March (Springer US, Boston, MA, 1983), p. 79.
[56] M. Ji, K. Umemoto, C. Z. Wang, K. M. Ho, and R. M. Wentzcovitch, Phys. Rev. B **84**, 220105 (2011).
[57] X. F. Zhao, X. Y. Yang, Y. X. Li, and R. Ahuja, J. Phys. Chem. C **124**, 22173 (2020).
[58] D. Le, T. B. Rawal, and T. S. Rahman, J. Phys. Chem. C **118**, 5346 (2014).
[59] R. Freitas and E. J. Reed, Nat. Commun. **11**, 3260 (2020).
[60] M. Neumann and O. Steinhauser, Chem. Phys. Lett. **106**, 563 (1984).
[61] R. Hou, Y. H. Quan, and D. Pan, J. Chem. Phys. **153**, 101103 (2020).
[62] E. Wasserman, B. Wood, and J. Brodholt, Geochim. Cosmochim. Acta **59**, 1 (1995).
[63] M. Chen *et al.*, Proc. Natl. Acad. Sci. U.S.A. **114**, 10846 (2017).
[64] O. Gereben and L. Pusztai, Chem. Phys. Lett. **507**, 80 (2011).
[65] C. J. Fennell, L. B. Li, and K. A. Dill, J. Phys. Chem. B **116**, 6936 (2012).
[66] M. L. Antipova and V. E. Petrenko, Russ. J. Phys. Chem. A **87**, 1170 (2013).
[67] H. K. Nienhuys, S. Woutersen, R. A. van Santen, and H. J. Bakker, J. Chem. Phys. **111**, 1494 (1999).
[68] C. J. Montrose, J. A. Bucaro, J. Marshall, and T. A. Litovitz, J. Chem. Phys. **60**, 5025 (1974).

[69] M. Nakahara, N. Matubayasi, C. Wakai, and Y. Tsujino, J. Mol. Liq. **90**, 75 (2001).
[70] R. Kumar, J. R. Schmidt, and J. L. Skinner, J. Chem. Phys. **126**, 204107 (2007).
[71] P. Schienbein and D. Marx, Phys. Chem. Chem. Phys. **22**, 10462 (2020).
[72] G. Berghold, C. J. Mundy, A. H. Romero, J. Hutter, and M. Parrinello, Phys. Rev. B **61**, 10040 (2000).
[73] A. Pasquarello and R. Resta, Phys. Rev. B **68** (2003).
[74] Y. S. Badyal, M. L. Saboungi, D. L. Price, S. D. Shastri, D. R. Haeffner, and A. K. Soper, J. Chem. Phys. **112**, 9206 (2000).
[75] K. Laasonen, M. Sprik, M. Parrinello, and R. Car, J. Chem. Phys. **99**, 9080 (1993).
[76] E. R. Batista, S. S. Xantheas, and H. Jonsson, J. Chem. Phys. **111**, 6011 (1999).
[77] L. Lodi, R. N. Tolchenov, J. Tennyson, A. E. Lynas-Gray, S. V. Shirin, N. F. Zobov, O. L. Polyansky, A. G. Császár, J. N. P. van Stralen, and L. Visscher, J. Chem. Phys. **128**, 044304 (2008).
[78] S. A. Clough, Y. Beers, G. P. Klein, and L. S. Rothman, J. Chem. Phys. **59**, 2254 (1973).
[79] I. Popov, P. Ben Ishai, A. Khamzin, and Y. Feldman, Phys. Chem. Chem. Phys. **18**, 13941 (2016).
[80] B. Guillot and Y. Guissani, J. Chem. Phys. **99**, 8075 (1993).
[81] G. S. Anderson, R. C. Miller, and A. R. H. Goodwin, J. Chem. Eng. Data **45**, 549 (2000).
[82] B. B. Owen, R. C. Miller, C. E. Milner, and H. L. Cogan, J. Phys. Chem. **65**, 2065 (1961).
[83] M. Ceriotti, J. Cuny, M. Parrinello, and D. E. Manolopoulos, Proc. Natl. Acad. Sci. U.S.A. **110**, 15591 (2013).
[84] A. I. Kolesnikov, G. F. Reiter, N. Choudhury, T. R. Prisk, E. Mamontov, A. Podlesnyak, G. Ehlers, A. G. Seel, D. J. Wesolowski, and L. M. Anovitz, Phys. Rev. Lett. **116**, 167802 (2016).
[85] X. Z. Li, B. Walker, and A. Michaelides, Proc. Natl. Acad. Sci. U.S.A. **108**, 6369 (2011).

Correction: Figures 1, 3, and 5 contained labeling errors and have been replaced. The angular brackets signifying averages were set improperly during the production cycle and have been set right.